Mon. Not. R. Astron. Soc. **000**, 1–16 (2016) Printed 5 January 2016 (MN LATEX style file v2.2)

Comparing Dark Energy Survey and HST–CLASH observations of the galaxy cluster RXC J2248.7–4431: implications for stellar mass versus dark matter

A. Palmese[1⋆], O. Lahav[1], M. Banerji[2], D. Gruen[3,4,5,6], S. Jouvel[1], P. Melchior[7], J. Aleksić[8], J. Annis[9], H. T. Diehl[9], T. Jeltema[10], K. Romer[11], E. Rozo[12], E. S. Rykoff[3,4], S. Seitz[5,6], E. Suchyta[13], Y. Zhang[14], T. M. C. Abbott[15], F. B. Abdalla[1,16], S. Allam[9], A. Benoit-Lévy[17,1,18], E. Bertin[17,18], D. Brooks[1], E. Buckley-Geer[9], D. L. Burke[4,3], D. Capozzi[19], A. Carnero Rosell[20,21], M. Carrasco Kind[22,23], J. Carretero[24,8], M. Crocce[24], C. E. Cunha[4], C. B. D'Andrea[19,25], L. N. da Costa[20,21], S. Desai[26,27], J. P. Dietrich[26,27], P. Doel[1], J. Estrada[9], A. E. Evrard[28,14], B. Flaugher[9], J. Frieman[9,29], D. W. Gerdes[14], D. A. Goldstein[30,31], R. A. Gruendl[22,23], G. Gutierrez[9], K. Honscheid[32,33], D. J. James[15], K. Kuehn[34], N. Kuropatkin[9], T. S. Li[35], M. Lima[36,20], M. A. G. Maia[20,21], J. L. Marshall[35], C. J. Miller[28,14], R. Miquel[37,8], B. Nord[9], R. Ogando[20,21], A. A. Plazas[38], A. Roodman[3,4], E. Sanchez[39], V. Scarpine[9], I. Sevilla-Noarbe[39,22], R. C. Smith[15], M. Soares-Santos[9], F. Sobreira[9,20], M. E. C. Swanson[23], G. Tarle[14], D. Thomas[19], D. Tucker[9], V. Vikram[40]

(Affiliations are listed at the end of paper)

5 January 2016

ABSTRACT

We derive the stellar mass fraction in the galaxy cluster RXC J2248.7–4431 observed with the Dark Energy Survey (DES) during the Science Verification period. We compare the stellar mass results from DES (5 filters) with those from the Hubble Space Telescope CLASH (17 filters). When the cluster spectroscopic redshift is assumed, we show that stellar masses from DES can be estimated within 25% of CLASH values. We compute the stellar mass contribution coming from red and blue galaxies, and study the relation between stellar mass and the underlying dark matter using weak lensing studies with DES and CLASH. An analysis of the radial profiles of the DES total and stellar mass yields a stellar-to-total fraction of $f_\star = (7.0 \pm 2.2) \times 10^{-3}$ within a radius of $r_{200c} \simeq 3$ Mpc. Our analysis also includes a comparison of photometric redshifts and star/galaxy separation efficiency for both datasets. We conclude that space-based small field imaging can be used to calibrate the galaxy properties in DES for the much wider field of view. The technique developed to derive the stellar mass fraction in galaxy clusters can be applied to the $\sim 100\,000$ clusters that will be observed within this survey. The stacking of all the DES clusters would reduce the errors on $f_\star$ estimates and deduce important information about galaxy evolution.

Key words: Dark Energy Survey – Clusters – Stellar Masses – Dark Matter – Photometric Redshifts.

⋆ E-mail:apalmese@star.ucl.uk

1 INTRODUCTION

In the last decade, large photometric galaxy surveys, such as SDSS, have provided us with a massive amount of data that have proven to be extremely useful for studies of cosmology. On the other hand, smaller area but deeper surveys like the Hubble Space Telescope (HST) based Cluster Lensing And Supernova Survey (CLASH) (Postman et al. 2012), allowed us to characterise single objects with unprecedented precision. The importance of finding synergies between these surveys relates to several aspects of observation (e.g. target selection, photometric calibration) and data analysis (photometric redshifts, physical properties of galaxies). This is particularly relevant for overlapping ground–based and space–based surveys: the higher quality that can be obtained from space can enable calibration and tests for the data collected by ground–based telescopes.

In this paper, we study the cluster of galaxies RXC J2248.7–4431 (RXJ2248 hereinafter). We make use of the synergies between DES and CLASH, and test in this way the performance of the early DES data at a catalog level (*i.e.* without making use of the images for the results). Photometric redshift (photo-z) and stellar mass results from CLASH are also used as a validation set for DES stellar mass estimates.

The aim of this paper is twofold: the first goal is to compare between DES's wide area breadth and CLASH's small area precision for the cluster RXJ2248. In fact, checks using HST data had not been done before to test the DES data, although the similar optical filters and the additional UV and IR HST bands make CLASH an optimal candidate for validation and quantifying uncertainties of photometry, photo-zs and stellar masses. The second is to illustrate how an analysis of the stellar mass distribution of this massive cluster over the wider Dark Energy Camera (DECam) field of view can be done.

In Section 2, we start by describing the two surveys considered. The cluster is described in Section 3. The comparison of DES and CLASH, in terms of photometric redshifts and star/galaxy separation, is presented in Section 4. Section 5 contains the second part of this paper, where we present the stellar mass results obtained from CLASH and DES, and compare the DES stellar masses to the total mass from the DES weak lensing analysis by Melchior et al. (2015). In the following, we assume a concordance ΛCDM cosmological model with $\Omega_m = 0.3$, $\Omega_\Lambda = 0.7$ and $h = 0.7$. In this cosmology, $1'$ corresponds to a physical transverse length of 295 kpc at the cluster redshift $z = 0.3475$.

The notation adopted in this paper for the cluster mass and radius follows the one often used in literature. The radii of spheres around the cluster centre are written as $r_{\Delta m}$ and $r_{\Delta c}$ where Δ is the overdensity of the sphere with respect to the mean matter density (subscript m) or the critical density (subscript c) at the cluster redshift. Masses inside those spheres are therefore $M_{\Delta m} = \Delta \frac{4\pi}{3} r^3_{\Delta m} \rho_m$ and similarly for $M_{\Delta c}$. In the following, we quote $\Delta = 200$, which is the density contrast at virialization for a dark matter halo.

2 DATA

The data used for the analyses developed for this paper come from DES and CLASH. The Dark Energy Survey is an optical-near infrared survey that is imaging 5000 deg^2 of the South Galactic Cap in the *grizY* bands over 525 nights spanning 5 years. The survey is being carried out using a new ~ 3 deg^2 CCD camera (the DECam, see Flaugher et al. 2015) mounted on the Blanco 4-m telescope at the Cerro Tololo Inter-American Observatory (CTIO) in Chile. DES started in 2012 with a testing period (November 2012 – February 2013) called DES Science Verification (SV). At the time of writing, two observing seasons (Diehl et al. 2014) have been completed, and a third is underway.

α_{J2000}	δ_{J2000}	Redshift	Luminosity (erg s^{-1})
22:48:44.29	-44:31:48.4	0.348	3.08×10^{45}

Table 1. Main properties of the cluster RXC J2248-4431. The quoted luminosity is in the rest frame 0.1-2.4 keV band.

The survey strategy is designed to optimize the photometric calibration by tiling each region of the survey with several overlapping pointings in each band. This provides uniformity of coverage and control of systematic photometric errors. This strategy allows DES to determine photometric redshifts of galaxies to an accuracy of $\sigma(z) \simeq 0.07$ out to $z \gtrsim 1$, with some dependence on redshift and galaxy type, and cluster photometric redshifts to $\sigma(z) \sim 0.02$ or better out to $z \simeq 1.3$ (The Dark Energy Survey Collaboration 2005). It will also provide shapes for approximately 200 million galaxies for weak lensing studies. For further information, see The Dark Energy Survey Collaboration (2005) or `www.darkenergysurvey.org`.

The fact that DECam has a ~ 3 deg^2 field of view gives us the opportunity of studying the large scale structure of galaxy clusters with only one pointing.

The cluster RXJ2248 was observed during the SV season, with typical exposure times of 90 seconds for the *griz* bands and 45 seconds for the Y band. It was re-observed later in 2013 to benefit from improvements to telescope performance and general image quality. The data reduction was done using the SVA1 DES Data Management (DESDM) pipeline, described in detail in Sevilla et al. (2011), Desai et al. (2012) and Mohr et al. (2012). The process includes calibration of the single-epoch images, that are then co–added after a background subtraction and cut into tiles. The SVA1 catalogue was created using SOURCE EXTRACTOR (SEXTRACTOR, Bertin & Arnouts 1996, Bertin & Arnouts 2010) to detect objects on the *riz* coadded images. The median 10σ depths of SV data are $g \sim 24.45, r \sim 24.30, i \sim 23.50, z \sim 22.90, Y \sim 21.70$, which reach close to the expected DES full depths. Limiting magnitudes were estimated for the 200 deg^2 SPT-E part of the wide–field SV area using BALROG (Suchyta et al. 2015) and PSF magnitude errors for true point sources.

We use AB magnitudes throughout this paper, and MAG_AUTO measurements given by SEXTRACTOR, as these proved to be robust and were thus used in several DES SV papers (e.g. Bonnett et al. 2015,Crocce et al. 2015). The objects selected for the analysis have a signal to noise $S/N > 10$ in the i band.

The other survey considered here is CLASH (Postman et al. 2012), a 524-orbit HST multi-cycle treasury program that has observed 25 massive clusters, having a range of

Survey/Instrument	Authors	FoV	Filters	Mag limits	Spectra	Objects
NTT+GMOS	Gómez et al. (2012)	$5' \times 5'$	V, R	–	116	711
CLASH	Postman et al. (2012), Monna et al. (2014)	$3.4' \times 3.4'$ (ACS), $2' \times 2'$ (WFC3)	16 in $2000 - 17000$ Å	$\sim$ 25-27 (10σ)	–	3471
WFI	Gruen et al. (2013)	$33' \times 33'$	$UBVRIZ$	26.4, 26.7 , 24.4 (VRI 5σ)	–	–
DES SV	Melchior et al. (2015)	$2.2\,\mathrm{deg}^2$	$grizY$	24.45, 24.30, 23.50, 22.90, 21.70 (10σ)	–	374 294

Table 2. Some experimental specifications of the surveys that have observed RXJ2248, with the corresponding paper in which those data have been used. The work presented in those papers is shortly summarised in Section 3. The magnitude limits reported for DES are the mean 10σ galaxy magnitudes.

virial masses[1] between $5 \times 10^{14} M_\odot$ to $30 \times 10^{14} M_\odot$ and an average redshift of $\bar{z} = 0.4$. The wavelength range covers the UV, the visible and the IR ($2000 - 17000$ Å) through 17 bands using the Advanced Camera for Surveys (ACS) and the Wide Field Camera 3 (WFC 3).

The CLASH mosaics were produced using the "MosaicDrizzle" pipeline (see Koekemoer et al. 2002, Koekemoer et al. 2011). The CLASH catalogue creation pipeline makes use of SExtractor: the software is run in dual image mode, where a detection image is created from a weighted sum of the ACS/WFC and WFC3/IR images. The WFC3/UVIS images are not used in the construction of the detection image but the UVIS data are still used to compute source photometry. The photometry given in the public catalogue (`http://www.stsci.edu/~postman/CLASH`), which is also the one used in this work, was measured in isophotal apertures, as they have been shown to produce reliable colours (Benítez et al. 2004). ACS/WFC3 reach a depth of 26.8, 26.4, 26.2, 26.0 and 26.6 (10σ galaxy AB magnitudes for circular apertures of 0.4 arcsec in diameter, Postman et al. 2012) in the F475W, F625W, F775W, F850LP and F105W filters, respectively.

Below, we compare the information obtained with 5 DES filters and with 17 HST filters.

3 THE CLUSTER RXC J2248.7–4431

In this section we present what is known about this cluster from previous works. The cluster of galaxies RXC J2248.7-4431, where RXC stands for ROSAT X-ray Cluster, is also known as Abell S1063 or MACS 2248-4431. It is a very luminous cluster, having an X-ray bolometric luminosity of $(6.95 \pm 0.1) \times 10^{45}$ erg s^{-1} in the energy range $0.1 - 100$ keV (Maughan et al. 2008). Its properties are listed in Table 1. It was first catalogued by Abell, Corwin & Olowin (1989), who counted 74 galaxies. Thanks to the ROSAT-ESO Flux Limited X-ray (REFLEX) Galaxy Cluster survey, Böhringer et al. (2004) measured a spectroscopic redshift $z = 0.3475$, which has been adopted in the recent literature and has also been confirmed in Gómez et al. (2012), who quoted a mean redshift of $z = 0.3461^{+0.0010}_{-0.0011}$ for 81 members.

Gómez et al. (2012) were the first to study in detail RXJ2248, even though it is the second most luminous cluster in the REFLEX survey (having a reported luminosity of $\sim 3.08 \times 10^{45}$ erg s^{-1} in the rest frame 0.1-2.4 keV band).

In Gómez et al. (2012), the cluster is presented as one of the hottest X-ray clusters known at that time. The high X-ray temperature, together with the high velocity dispersion, suggest a very massive cluster ($M_{200c} > 2.5 \times 10^{15} M_\odot$) and/or a merger system. The merger model is supported by a small offset between the galaxy distribution and the peak of X-ray isophotes, and a non-Gaussian galaxy velocity distribution. Gómez et al. (2012) also reported that the velocity distribution is better represented by the velocity dispersion produced during a merger than by the velocity distribution of a relaxed cluster.

Gruen et al. (2013) use Wide-Field Imager (WFI) data to perform a weak lensing analysis of the cluster. They parametrised the cluster density with a NFW profile (Navarro, Frenk & White 1996) and obtained a mass $M_{200m} = 33.1^{+9.6}_{-6.8} \times 10^{14} M_\odot$. They also identify a second galaxy cluster in the field of view at redshift ~ 0.6, with an estimated mass of $M_{200m} = 4.0^{+3.7}_{-2.6} \times 10^{14} M_\odot$.

Melchior et al. (2015) studied the weak lensing masses and galaxy distributions of four massive clusters observed during the DES SV period, including RXJ2248. They find $M_{200c} = 17.5^{+4.3}_{-3.7} \times 10^{14} M_\odot$, which is in agreement with previous mass estimates. For RXJ2248, they also identified filamentary structures of the luminous red-sequence galaxies found with the RedMaPPer (Rykoff et al. 2014) algorithm.

4 COMPARISON OF DES AND CLASH

In this section, we assess detectability, photometry, and stellar masses of DES galaxies, treating matched CLASH galaxies as truth table.[2] In order to make the comparison, we seek to identify similar filters in both data sets. Figure 2 shows that the closest HST analogs to DES $griz$ are F475W, F625W, F775W and F850lp. We will refer to the corresponding HST and DES bands as g, r, i and z for simplicity of notation. In the following, we will also use the DES Y band, that does not have a similar HST filter. When we refer to 5

[1] The virial mass is usually taken as M_{200c}.

[2] A comparison of weak lensing measurements between DES and CLASH was not performed because they predominantly reveal differences in the shear calibration. The majority of galaxies with shape measurement in both catalogs are very faint for DES, resulting in large and noisy calibration factors (see Section 4.2.1 in Melchior et al. 2015). In addition, the high density of galaxies in the central region of this cluster creates many more close galaxy pairs or even blends in ground–based DES images than when viewed with HST, rendering shape measurement even more challenging. A detailed analysis of those relevant effects is beyond the scope of this paper.

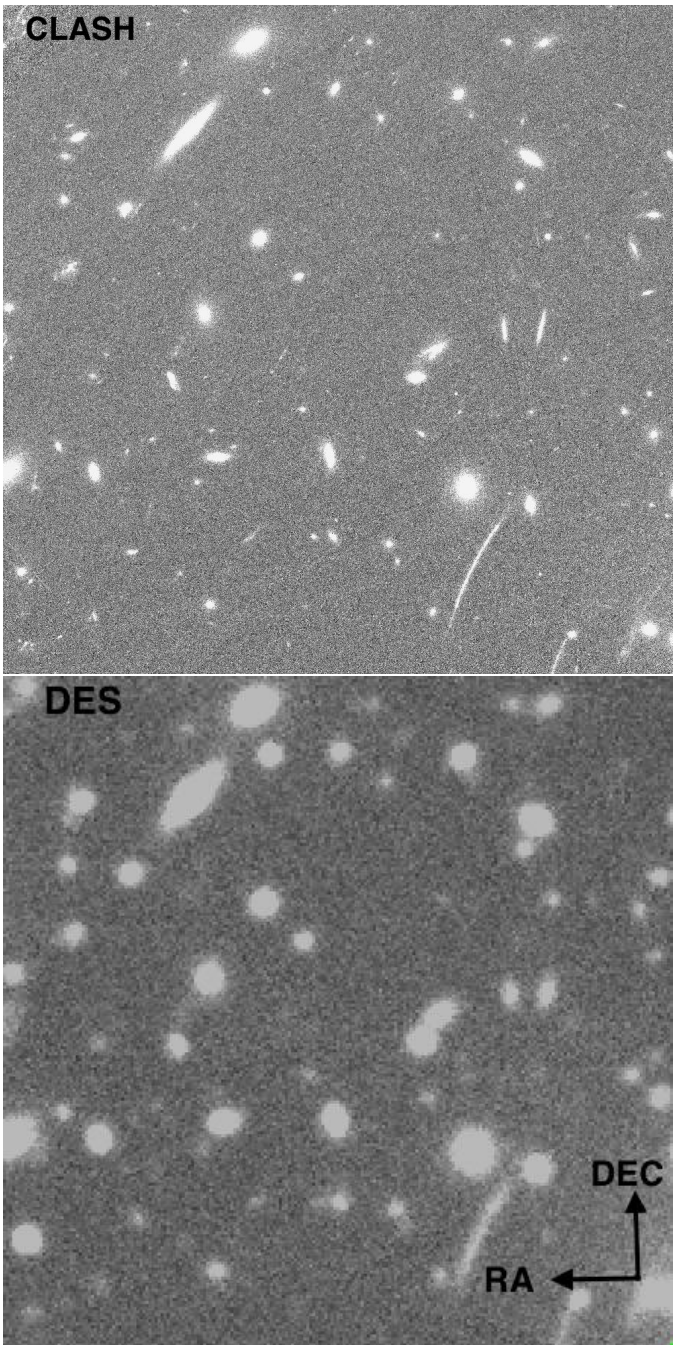

Figure 1. A portion of $1' \times 1'$ image centered in RA 22:48:48.003 and DEC -44:31:38.52 in the CLASH F625W band (top) and the DES r band (bottom).

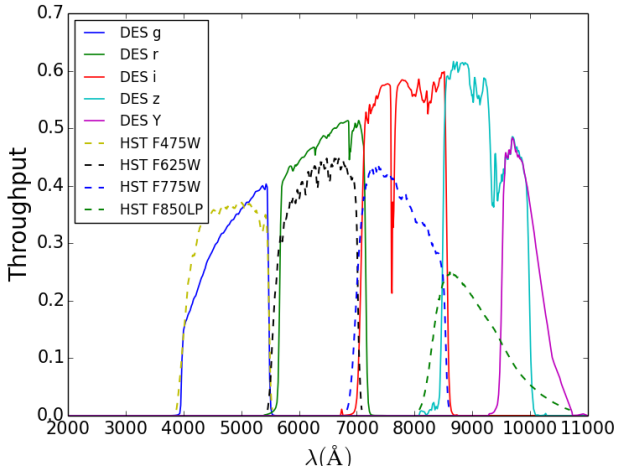

Figure 2. Throughput of the DES filters (solid lines) and HST similar filters (dashed lines).

CLASH filters, it means we are including the F105W filter, that is broader than the DES Y.

In the DES catalogue of the RXC J2248.7-4431 area, there are 374 294 sources in a roughly circular area of approximately 3 deg^2. The deeper, higher resolution CLASH catalogue includes 3 471 sources in a much smaller area ($\sim 5' \times 4'$).

We perform a spatial matching (using a matching radius of 1.5″) between the DES and CLASH catalogues and we find 609 matched sources. Thus the DES recovered only 18% of the sources in the CLASH catalogue. The high percentage of sources missed in DES is due to various problems, one of them being that the *griz* 10σ depths differ by $\gtrsim 2$ magnitudes between the two datasets. This accounts for most of the undetected sources in DES: when we simulate fake faint galaxies with BALROG[3] (Suchyta et al. 2015) on the DES image of RXJ2248, we find that the completeness in *riz* bands (which are those used to run the detection) drops below 20% between magnitude 24 and 25, justifying the incompleteness found when comparing to the even deeper CLASH survey. We also expected one of the problems to be blending, especially close to the bright cluster core. We run some completeness tests using a DES enhanced deblending catalogue (Zhang et al. 2014) that would increase the percentage of recovered sources to 20%, but found that blending is not a major reason of incompleteness. Also, CLASH object detection is run on ACS+IR images, while DES detection only involves optical bands and it may miss redder sources.
A visual comparison of DES and CLASH images is shown in Figure 1.

A comparison of measured isophotal magnitudes at the catalogue level between the matched galaxies in the two datasets here considered shows a mean shift $|\Delta m| \leqslant 0.13$ in all bands, where the offsets due to the different filters compared have been taken into account. This is true when a signal to noise cut $S/N > 10$ is performed on the matched galaxies, and objects with saturated pixels and corrupted DES data are removed. A magnitude analysis is presented in Appendix A.

4.1 Star/galaxy separation

For the purpose of studying the star/galaxy separation, we adopt the same notation used in Soumagnac et al. (2013). We study the galaxy completeness c_g, defined as the ratio of the number of true galaxies classified as galaxies to the total number of true galaxies (including then also the number of true galaxies classified as stars M_G):

[3] A software pipeline for embedding simulations into astronomical images. `https://github.com/emhuff/Balrog`

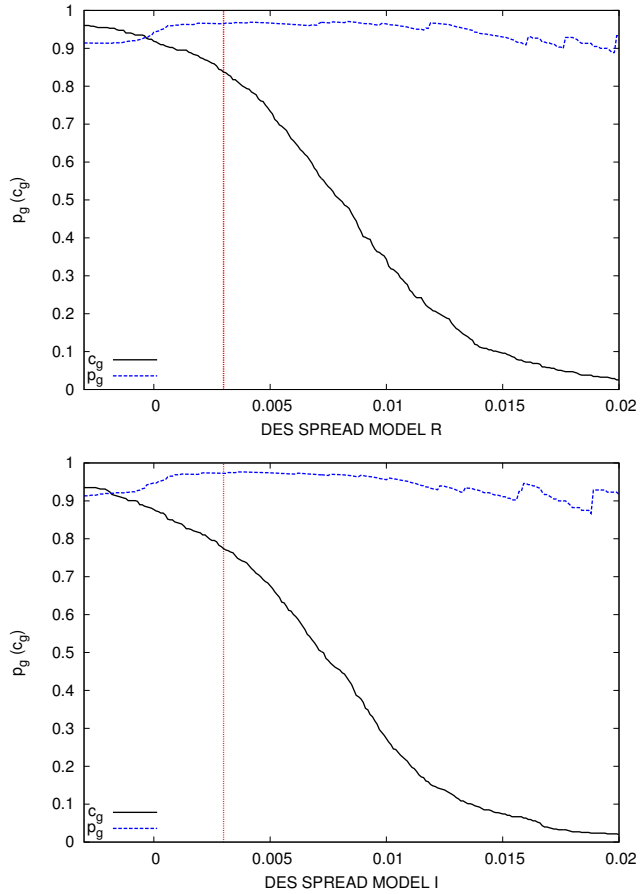

Figure 3. Galaxy purity (blue dashed line) and completeness (black solid line) for the star/galaxy separation problem using the `SPREAD_MODEL` parameter in the DES catalogue for the r (top) and i (bottom) bands. The red vertical line represents a typical cut used for `SPREAD_MODEL`, which is 0.003.

$$c_g = \frac{N_G}{N_G + M_G} \ , \tag{1}$$

where here N_G is given by the galaxies in the DES catalogue, and the number of true galaxies is given by the object classified as such in CLASH.
Moreover the galaxy purity p_g is defined as

$$p_g = \frac{N_G}{N_G + M_S} \ , \tag{2}$$

where M_S is the number of stars classified as galaxies.

We consider as true galaxies the sources that have a SExtractor stellarity index `CLASS_STAR`< 0.08 in the CLASH catalogue, otherwise they are stars. This cut on the CLASH has been proven to perform well in other CLASH works (e.g. Jouvel et al. 2014). We try to understand if the star/galaxy performance is compatible between the two datasets.

We first consider the `CLASS_STAR` parameter given in the DES catalogue. We find that a cut between 0.7 and 0.9 for the `CLASS_STAR_I` gives purity and completeness above the 90%. The number of galaxies and stars in the two catalogues can be found in Table 3.

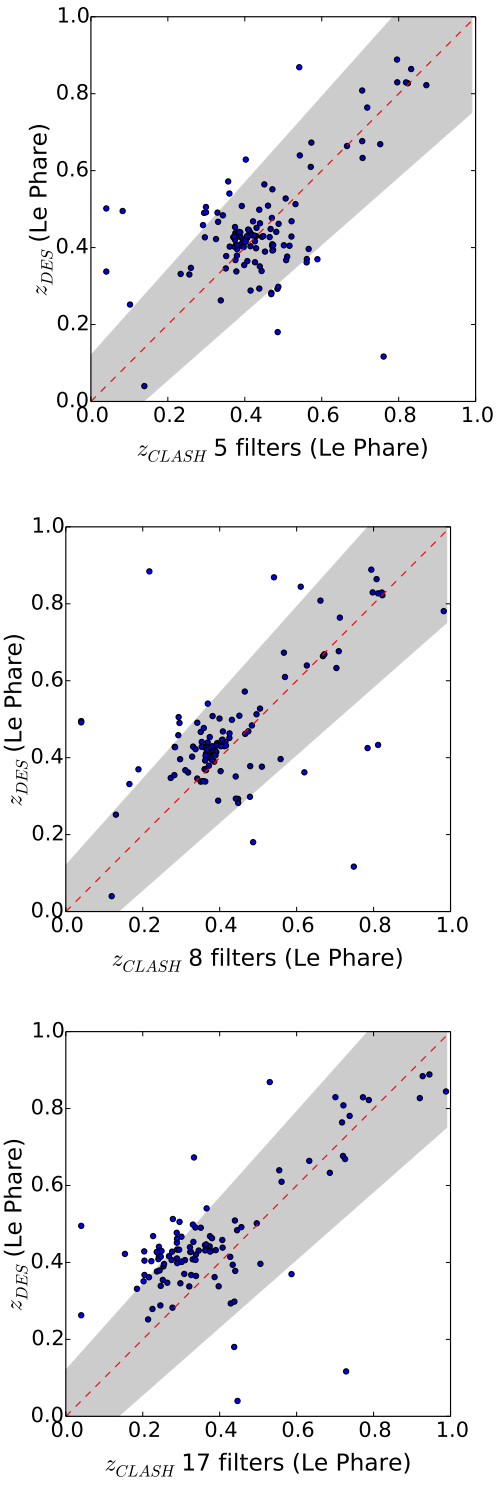

Figure 4. Comparison of the DES versus CLASH photo-zs for the sources matched between the two catalogues. Photo-zs were obtained using LePhare. *Top:* only the 5 HST filters similar to the *grizY* filters in DES have been used to compute CLASH photo-zs. *Middle:* 3 of the HST UV filters have been added to the 5 HST optical filters for the CLASH photo-z estimation. *Bottom:* all the 17 available CLASH filters have been used to estimate the photo-zs. The red dashed line represents $z_{DES} = z_{CLASH}$, and the grey area the expected DES accuracy of $|z_{DES} - z_{CLASH}| < \sigma(1 + z_{CLASH})$, where $\sigma = 0.12$.

CLASS_STAR	g	r	i	z
G(DES)	551	538	535	522
G(CLASH)	553	553	553	553
S(DES)	58	71	74	87
S(CLASH)	56	56	56	56
SPREAD_MODEL	g	r	i	z
G(DES)	388	463	428	405
G(CLASH)	553	553	553	553
S(DES)	221	146	181	204
S(CLASH)	56	56	56	56

Table 3. Number of galaxies G and stars S found in DES and CLASH, when considering CLASS_STAR < 0.8 (top table) and SPREAD_MODEL > 0.003 (bottom table) for galaxies in DES.

We also test the performance of star/galaxy separation with the SPREAD_MODEL parameter (defined in Desai et al. 2012 and tested in Bouy et al. 2013). SPREAD_MODEL is a morphological star/galaxy separation parameter given by SExtractor which acts as a linear discriminant between the best fitting local PSF model and a slightly "fuzzier" version made from the same PSF model, convolved with a circular exponential model. A threshold is set to 0.003 by the DESDM pipeline to separate stars (PSF like, having absolute values below 0.003) from galaxies (non-PSF like, with values higher than 0.003). As a result, 77.4% of the galaxies are catalogued in DES as such, and the purity is 97.3%. A plot for the purity and the completeness for varying SPREAD_MODEL_I cuts is shown in Figure 3. We list the number of galaxies and stars in the two catalogues in Table 3. It can be seen from Figure 3 that cut at lower values ($\sim 0.001 - 0.002$) would give a higher completeness without affecting the purity significantly. Moreover, in this case may be better using the SPREAD_MODEL in the r band, which is deeper than the i one, and this can also be seen in Figure 3, where it is clear that, for the same cut, the completeness is higher. We also find that using the CLASS_STAR parameters with the mentioned cut is more efficient than adopting the SPREAD_MODEL_I with the cut at 0.003.

4.2 Photo-z

Considering only those matched sources with a signal to noise ratio $S/N > 10$ in the DES i-band, excluding stars (in this case we exclude all objects with CLASS_STAR_I> 0.8) and objects with FLAGS $\neq 0$ (in order to exclude objects with saturated pixels or corrupted data, and originally blended sources) we are left with 155 sources. This is the subset of galaxies that we will use for the photo-z and stellar mass comparison.

In order to estimate the photo-zs, we used the publicly available software LePhare (Arnouts et al. 1999, Ilbert et al. 2006)[4], as it also produces the stellar masses that we want to study in this paper. Previous works on DES photo-zs (Sánchez et al. 2014) have tested the performance of this code in comparison with other softwares and spectroscopic redshifts, but stellar masses tests have not been performed with DES data so far. We therefore need to further check the DES photo-z and stellar mass estimation with LePhare first. This is where the HST data are particularly useful in this work, as we need to check DES against a more precise photometric survey covering the wavelengths from optical to IR.

Furthermore, LePhare is a reliable code, as seen in e.g. Ilbert et al. 2009.

4.2.1 LePhare *photo-z technique*

The main purpose of LePhare is to compute photometric redshifts by comparing template Spectral Energy Distributions (SEDs) to the observed broadband photometry, but it can also be used to calculate physical parameters such as stellar masses and rest-frame luminosities. Several SEDs sets are available within the code, and these are redshifted and integrated through the instrumental transmission curves. Additional contribution of emission lines in the different filters can be included and extinction by dust can be taken into account. The synthetic colours obtained from the SEDs for each redshift are then compared to the data. The best fitting template and redshift for each object is then found by χ^2 minimisation. In addition, prior information can be supplied, including a photo-z distribution prior by galaxy type computed from the VVDS survey in the i band (see Ilbert et al. 2006).

4.2.2 Results

We run LePhare on both CLASH (with 5, 8 and all 17 filters) and DES (5 filters) catalogues, fitting the 31 synthetic SEDs templates given by the COSMOS (see Ilbert et al. 2009) libraries. We use four galaxy extinction values ranging from 0.05 to 0.3 using a Calzetti et al. (2000) extinction law for DES. For CLASH, two more extinction values are added (0.4 and 0.5), in order to take into account the wider wavelength range covered when we use all its filters.

The results are plotted in the upper panel of Figure 4 for the 155 matched sources when 5 filters are considered for CLASH. Of all the sources considered, 85% have a photo-z which is compatible with the CLASH photo-z within the DES requirement[5] $|z_p - z_s| < \sigma(1 + z_s)$, where $\sigma = 0.12$. We notice an offset in the CLASH redshift when 17 filters are used (see lower panel of Figure 4), while 77% of the sources still satisfies the DES requirement. This mostly likely stems from the inclusion of near-UV filters to get an accurate redshift from the Balmer break for galaxies below a redshift of 0.4 (see e.g. Eisenstein et al. 2001). In fact, this offset starts to be seen also when adding only three UV bands (namely F336W, F390W and F435W) to the $grizY$ filters (see middle panel in Figure 4).

Zero points[6] have not been adopted in the DES photo-z estimation, as we saw that their introduction causes systematic effects. Zero points are calculated using

[4] http://www.cfht.hawaii.edu/~arnouts/LEPHARE/lephare.html

[5] Where z_p and z_s are the photometric and spectroscopic redshifts, so here we consider the CLASH photo-z as the "spectroscopic" one.

[6] Zero–points define the shift in the observed magnitudes due to various systematics.

field galaxies, so we believe we would need spectroscopy in the cluster field to be helpful at photo-z calibrations for this study.

4.3 Stellar Masses

Stellar masses are key observables in the study of galaxy evolutionary models. Unfortunately, they cannot be directly measured, but require multicolour photometry to be fitted with stellar population models, therefore making a series of assumptions. One of these is the galaxy redshift if spectroscopy is not available: in the view of our goal of computing the stellar mass profile of the RXJ2248 cluster, we have to bear in mind that galaxy redshift accuracy is essential not only to ensure the correct template match in the template fitting method here used and the distance to the galaxy, but also to determine the cluster membership. We will therefore see how the redshift assumptions affect the stellar mass estimation and elaborate a reasonable technique to correctly estimate the stellar mass profile.

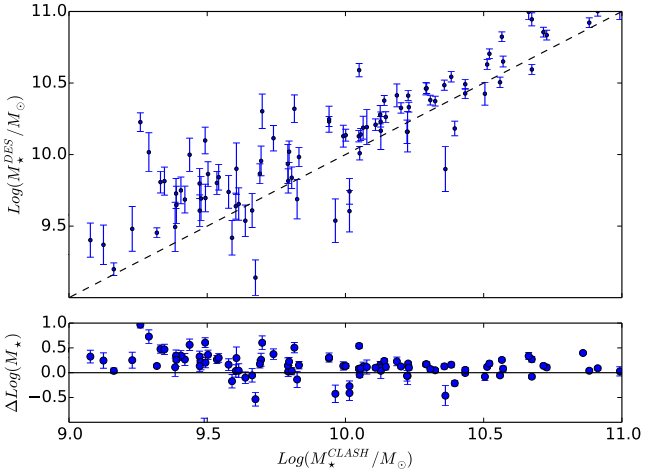

Figure 5. DES stellar masses versus CLASH stellar masses computed using LePhare. In the stellar mass estimation, each source is assumed to be at the redshift given as output by LePhare, as described in Section 4.2. The dashed line line represents $M_\star^{DES} = M_\star^{CLASH}$. In the bottom panel $\Delta Log(M_\star) = Log(M_\star^{DES}) - Log(M_\star^{CLASH})$ is presented. All available filters (*i.e.* 5 for DES and 17 for CLASH) have been used in the estimation process. Uncertainties represent the 68% Confidence Level.

4.3.1 Method

We use the same sample of matched galaxies with $S/N > 10$ used in Section 4.2 and their redshift estimations in order to compute the stellar masses for both DES and CLASH using LePhare. In the first place, the redshifts of the galaxies are fixed to those photo-zs previously computed (*i.e.* to DES photo-zs for DES stellar masses, and to CLASH photo-zs for CLASH stellar masses). In the second case, we fix the galaxy redshifts at the cluster redshift for both DES and CLASH, and the LePhare DES photo-zs are only used to select a subsample of cluster members satisfying $|z_{phot} - z_{cl}| \leqslant 0.12$. For this subsample both DES and CLASH stellar masses are estimated.

We chose to use LePhare, together with the Bruzual & Charlot (2003) templates, as this combination has been shown to be robust in the estimation of physical parameters of galaxies (Ilbert et al. 2010).

We derive our stellar mass estimates by fitting synthetic SEDs templates while keeping the redshift fixed as described previously in the two cases. The SED templates are based on the stellar population synthesis (SPS) package developed by Bruzual & Charlot 2003 (BC03) assuming a Chabrier (2003) initial mass function (IMF). Our initial set of templates includes 9 models using one metallicity ($Z = 1Z_\odot$) and nine exponentially decreasing star formation rates $\propto exp(-t/\tau)$ where t is the time and τ takes the values $\tau = 0.1, 0.3, 1, 2, 3, 5, 10, 15, 30$ Gyr. The final template set is then generated over 57 starburst ages ranging from 0.01 to 13.5 Gyr, and four extinction values ranging from 0.05 to 0.3 using a Calzetti et al. (2000) extinction law. For CLASH, two more extinction values are added (0.4 and 0.5).

The uncertainties on our stellar masses estimates (`MASS_BEST` from LePhare) are given by the 68% confidence limits on the SED fit.

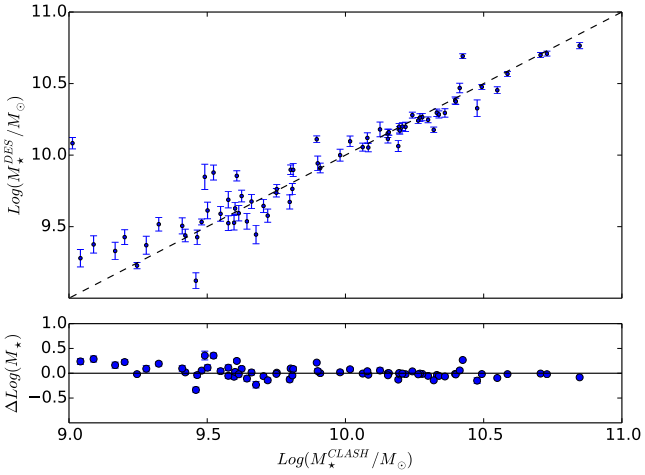

Figure 6. DES stellar masses versus CLASH stellar masses computed using LePhare. Here only sources around the cluster redshift are considered (*i.e.* sources with a DES photo-z that satisfies $|z - z_{cl}| \leqslant 0.12$, where $z_{cl} = 0.3475$ is the cluster redshift). In the DES and CLASH stellar mass estimation, these galaxies are all assumed to be at z_{cl}. The dashed line line represents $M_\star^{DES} = M_\star^{CLASH}$. In the bottom panel $\Delta Log(M_\star) = Log(M_\star^{DES}) - Log(M_\star^{CLASH})$ is presented. The offset seen in Figure 5 seems to disappear in this plot, showing that this effect was due to the photo-z offset. All available filters (*i.e.* 5 for DES and 17 for CLASH) have been used in the estimation process. Uncertainties represent the 68% Confidence Level.

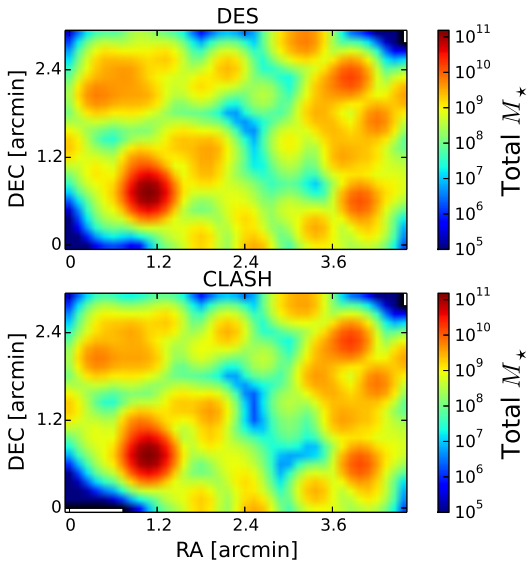

Figure 7. DES and CLASH total stellar mass maps computed using LePhare for the galaxies matched between the two catalogues. The stellar masses plotted are the same as those shown in the bottom panel of Figure 6 (*i.e.* all the galaxies with a DES photo-z that satisfies $|z - z_{cl}| \leqslant 0.12$, where z_{cl} is the cluster redshift, have a redshift fixed to z_{cl} in the SED fitting). The map is centred on the BCG, but its stellar mass is not visible as it was originally blended and therefore did not pass the quality flag cut applied in Section 4.3. The resolution is $0.12'$/pixel and the map is smoothed with a Gaussian of $\sigma = 0.144$ arcmin. At the cluster redshift, $1'$ corresponds to 294 kpc in the assumed cosmology.

4.3.2 Results

In Figure 5, we show the comparison between DES and CLASH stellar mass estimates for the first case, where the redshifts are fixed to the LePhare estimates. The linear correlation between the two estimates is clear, but there is an offset of mean value ~ 0.16 dex. This should be considered in light of two aspects:

(i) the offset in the photo-zs that we addressed in Section 4.2;
(ii) the uncertainties in the DES stellar masses may be underestimated as those are the 68% confidence limits on the SED fit and do not take into account systematic error contribution.

In Figure 6 we show the results for the second case, where we select the galaxies with a DES photo-z close to the spectroscopic cluster redshift z_{cl}, satisfying $z_{cl} - 0.12 < z_{phot} < z_{cl} + 0.12$. The redshift of these sources is fixed at z_{cl} in the stellar mass estimation, and the reason for this choice is twofold:

(i) to minimise circularity associated with using LePhare to both measure redshifts and stellar masses;
(ii) to take into account the shift in the redshift estimates pointed out in Section 4.2 (and therefore put at the correct cluster redshift the cluster members which photo-z appeared to be at $z_{phot} \sim 0.4$).

Of course this choice results in considering some sources as being at z_{cl} even though they are not, and we shall take this into account in the following. A consistency test for the choice of redshifts that has been made is presented in Appendix B.

The correlation between the estimated stellar masses significantly increases if also the CLASH sources are set to be at the cluster redshift, as seen in a comparison of Figure 5 with Figure 6, where we find that stellar masses from DES can be estimated within 25% of CLASH values. This shows that the offset seen in the former is due to the offset in the redshifts given in input, rather than other systematics. Therefore, the wavelengths covered by the DES broadband filters are capable of providing a good estimation of stellar mass if the photometric redshift is sufficiently precise.

In Figure 7 we show the spatial distribution of the total stellar mass spatial distributions for both DES and CLASH in the CLASH field ($\sim 4.8' \times 4.2'$), represented with a resolution of $0.12'$/pixel and smoothed with a Gaussian of $\sigma = 0.144$ arcmin. The stellar masses of galaxies are summed over in each pixel. Obviously that the two samples show very good agreement in terms of the spatial distribution of stellar mass.

5 DARK MATTER AND STELLAR MASSES

In this section we study the stellar mass radial profile of the cluster and relate it to that of dark matter that has been obtained though DES weak lensing studies in Melchior et al. (2015). As shown in Section 4.3, stellar mass estimation can be biased if the redshift assumed is biased too: this is a problem if one wants to compute stellar masses with photometric surveys data. In the lack of spectroscopy, it is a common method to perform estimation of the photometric redshift and SED fitting in two steps, which involve fixing the redshift of a galaxy at the best fit value obtained in the first step. Although this may not be the most elegant way of solving the problem, it has been proven to lead to only a small bias in the SED fitting parameters, when compared to results given by the simultaneous estimation of redshift and stellar mass (see Acquaviva, Raichoor & Gawiser 2015). Nevertheless, here we want to adopt a more consistent methodology for the stellar mass estimation, taking advantage of the fact that we are looking at a cluster with a known redshift. This technique is outlined in the first part of this section, followed by a study of the different mass radial profiles obtained. To allow a straightforward comparison with the weak lensing reconstructed mass, we compute total stellar mass and surface density on a projected 2-dimensional plane, i.e.:

$$M_\star(R) = \sum_i m^i_\star \qquad \Sigma_\star(R) = \frac{\sum_i m^i_\star}{A_{\rm annulus}}\,, \tag{3}$$

where the sums are intended over the galaxies within annuli of projected radius R. Similar definitions apply for the cumulative distributions $M_\star(< R)$ and $\Sigma_\star(< R)$, computed within circles of radius R. The centre of the image is taken to be that of the BCG. At last, we present a comparison between the stellar and total DES mass maps.

5.1 Galaxy samples and stellar mass estimates

Our goal is to compare the reconstructed mass from weak lensing to the total stellar mass of the cluster members. In order to do so, we split the galaxies into two populations. The following steps are performed:

- We select the red members using the REDMAPPER SV catalogue (Rozo et al., in prep.), which identifies cluster members with high precision (Rozo et al. 2014). Their stellar masses are computed using the same parameters presented in Section 4.3 (but fixing the redshift at z_{cl}).
- The RedMaPPer galaxies profile has been corrected by a factor representing the contribution coming from faint sources at luminosities smaller than the limit of the sample ($0.2L^*$). This is done by integrating the luminosity with a Schechter function, *i.e.* we computed the fraction:

$$F_L = \frac{\int_0^{0.2L^*} L\phi(L)dL}{\int_0^{\infty} L\phi(L)dL}\,, \tag{4}$$

where $\phi(L) = \phi_*(\frac{L}{L^*})^{\alpha}e^{-L/L^*}$ with $\alpha = -1$ (as done in Rykoff et al. 2014 for the SDSS sample, that has properties similar to DES). We find that the galaxies below the luminosity limit contribute to a fraction $F = 0.18$ of the total luminosity, and therefore, assuming a constant $M_\star/L$ ratio for the red galaxy population, they contribute to the same percentage of stellar mass.
- The contribution to the total stellar mass of each red member is weighted by its membership probability (reported in the RedMaPPer catalogue).
- In order to study the mass profile at radii higher than r_{200c}, we decide not to neglect the contribution coming from the bluer population. First, we exclude all objects with saturated pixels or corrupted data, but include galaxies that were initially blended (such as the BCG). Then we select the rest of the galaxies in the field of view that have magnitudes m_i in the i band satisfying $m_i^{\rm BCG} < m_i < m_i^{\rm lim}$. In this way we exclude any source which is brighter than the BCG and cut at $m_i^{\rm lim} = 21$ mag in order to ensure the completeness of the sample. After having performed a SED fitting as in the previous step, we filter out all galaxies that do not give a good fit (cutting on reduced $\chi^2 < 2$) when the redshift is fixed at the cluster value.

5.2 Masking and background correction

We estimate the survey area lost due to masked regions and blending of faint galaxies with large cluster members near the core. We calculate corrections for both effects as follows.

- HEALPIX (Górski et al. 2005) maps of depth and masking fractions are produced for DES with MANGLE (Swanson et al. 2008). From these, we calculate mean depth and fractions of masked area in our set of annuli. The depth is approximately constant out to ≈ 50 arcmin from the BCG, which defines the outer limit of the area used for our background estimation scheme. Masking fractions are below 5 per cent for all annuli and applied to the binned stellar mass estimates from both galaxy samples.
- For the blue galaxy sample, some objects are lost due to blending with cluster member galaxies. Without correction, this would bias our stellar mass estimates of blue galaxies near the cluster centre low. We estimate the area lost in each annulus as the isophotal area above the SEXTRACTOR detection threshold, `ISOAREA_I`. This yields a ≈ 7 per cent correction in the innermost arcminute, which drops quickly towards larger radii. For the blue galaxy sample, this correction and the masking fraction are applied in an additive fashion.

The contribution coming from galaxies that do not actually sit at the cluster redshift is removed from the blue galaxies sample by performing a background subtraction: we estimate the projected surface density of the stellar mass $\Sigma_\star(R)$ at large radii ($30 - 50$ arcmin, which means outside $\approx 3r_{200c}$ [7]), where the stellar mass profile tends to become flat. The value found is $\Sigma_\star = 1.36 \times 10^{10} M_\odot/\mathrm{arcmin}^2$ and this is subtracted on the smaller scales, with an uncertainty given by a Poissonian error. The remaining stellar mass contribution is then added to that of the red galaxies.

5.3 Stellar mass profile

We look at the radial distribution of stellar mass, taking into account both the red cluster members present in the REDMAPPER catalogue, and the blue members, as explained in the previous section. The choice of subtracting the background contribution from the stellar mass profile is also justified in light of the stellar mass to total mass comparison: the weak lensing signal suffers from the mass sheet degeneracy, so subtracting any constant contribution is consistent. The final $\Sigma_\star(R)$ profile for the non–RedMaPPer sample that is left after the background subtraction provides a good estimate of the contribution to stellar mass coming from the blue cluster members. Moreover, the splitting into red and blue galaxies is justified by the possibility of improving the SED fitting by using different priors for the two populations, and considering the systematics differently. In fact, it is well known that stellar masses estimated for quiescent galaxies are more reliable than for star-forming ones, partially because the colour–$M_\star/L$ (from which $M_\star$ is derived) relation are more uncertain for very blue colours (see e.g. Conroy 2013 and Banerji et al. 2013).

The total stellar mass cumulative profiles $M_\star(< R)$ for the red and blue galaxies are shown in Figure 8. Within the innermost 5 arcmin, the contribution of the red cluster members to the total stellar mass is dominant ($\gtrsim 80\%$) with respect to the bluer galaxies, while at larger radii, namely outside r_{200c}, the second population considered gives a $20 \ldots 50\%$ contribution to the total stellar mass. In Figure 8 we also plot the stellar mass profile from CLASH, where the galaxy cluster members were selected cutting on the CLASH photometric redshift with $|z_{phot} - z_{cl}| < 0.12$.

5.4 Comparison to total mass from Weak Lensing

The weak lensing mass profile is computed through the aperture mass densitometry (see Meneghetti et al. 2010) using $M_{tot}(< R) = \pi R^2 \bar{\kappa}(< R)\Sigma_{cr}(z_l, z_s)$, where $\bar{\kappa}(< R)$ is the mean convergence within a circular aperture of radius R, z_l and z_s are the redshift of lens and sources. The convergence

[7] $r_{200c} = 3150$ kpc from the NFW fit of Gómez et al. 2012, which means $r_{200c} \simeq 10.7'$ at the cluster redshift

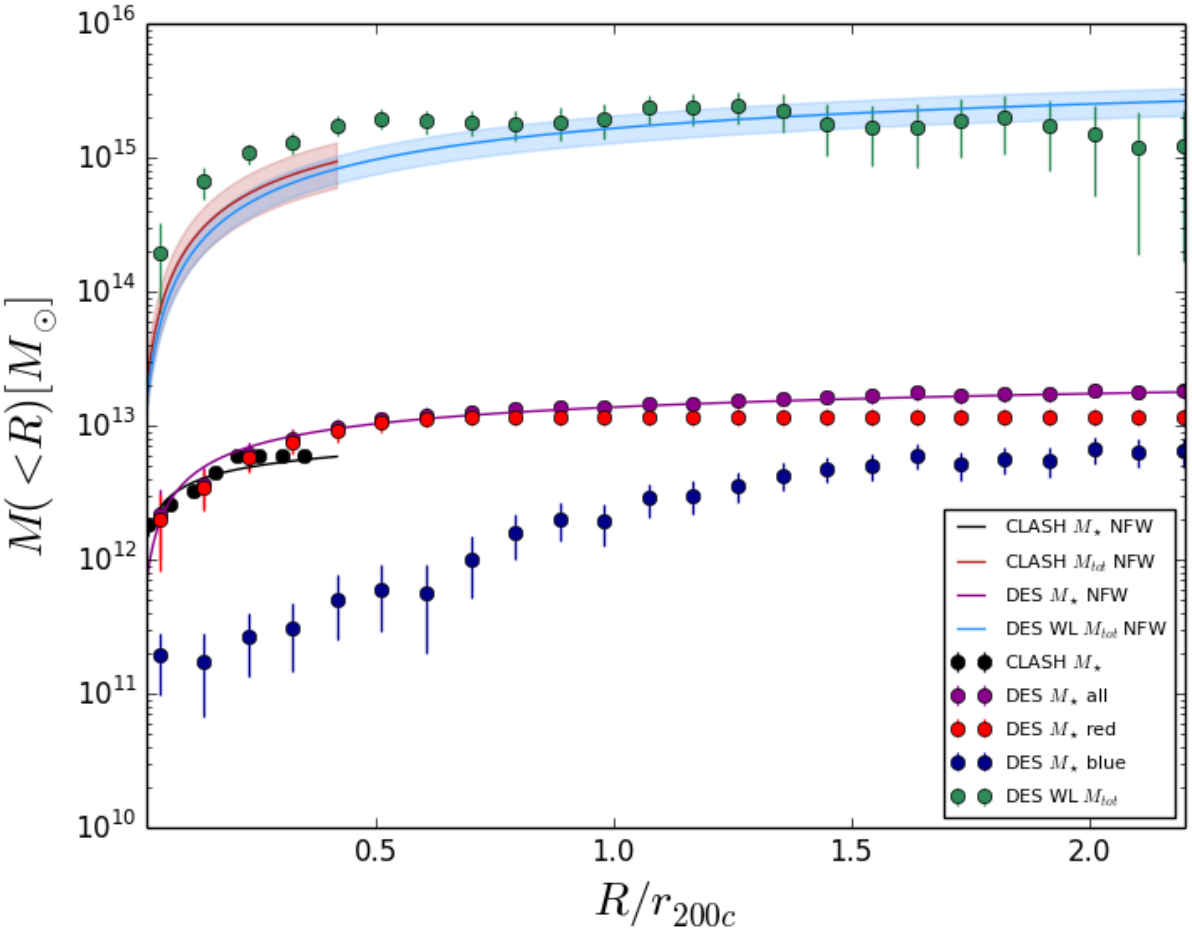

Figure 8. Cumulative radial distributions of total stellar mass derived in this paper for the DES red (red points), blue (blue points) and all galaxies (purple points) in the cluster, together with the total, non-parametric mass profile reconstructed from DES weak lensing (Melchior et al. 2015, green points). The purple solid line is our NFW fit to the DES stellar mass profile, while the blue solid line is the NFW best fit from DES weak lensing. The black points represent the CLASH total stellar mass profile computed in this paper, with our NFW fit (black solid line). The red solid line is the Umetsu et al. (2015) NFW best-fit for CLASH from a strong lensing, weak lensing and magnification joint analysis. The radius R is projected, and $r_{200c} = 3.15$ Mpc. Errorbars show the 68% confidence level.

κ is defined as the projected surface mass density Σ, in units of the critical surface mass density Σ_c:

$$\kappa = \frac{\Sigma}{\Sigma_c}\,, \qquad \Sigma_c = \frac{c^2}{4\pi G}\frac{D_s}{D_d D_{ds}} \tag{5}$$

where D stands for angular diameter distance and the subscripts s, d, ds indicate the distance from the observer to the source, from the observer to the lens, and from the lens to the source respectively.

In Figure 8 we present the NFW mass profile derived by using the best fit parameters as found in Melchior et al. (2015) for this cluster. Given the similarity between the WL and stellar mass profiles, we try to fit the stellar mass one with a NFW projected mass profile, as the one derived in e.g. Oaxaca Wright & Brainerd (1999):

$$M(<x) = \begin{cases} \frac{3\delta_c M_{200c}}{200 c_{200}^3}\left[\frac{2}{\sqrt{1-x^2}}\operatorname{arctanh}\sqrt{\frac{1-x}{1+x}} + \ln(\frac{x}{2})\right] & (\text{if } x<1) \\ \frac{3\delta_c M_{200c}}{200 c_{200}^3}\left[1+\ln(\frac{1}{2})\right] & (\text{if } x=1) \\ \frac{3\delta_c M_{200c}}{200 c_{200}^3}\left[\frac{2}{\sqrt{x^2-1}}\arctan\sqrt{\frac{x-1}{1+x}} + \ln(\frac{x}{2})\right] & (\text{if } x>1) \end{cases} \tag{6}$$

where $x = R/r_s$, $c_{200} = r_{200}/r_s$ is the concentration parameter and

$$\delta_c = \frac{200}{3}\frac{c_{200}^3}{\ln(1+c_{200}) - c_{200}/(1+c_{200})}\,. \tag{7}$$

Our non-linear least squares fit uses the Levenberg-Marquardt algorithm and gives the following parameters for DES stellar mass profile: $M_{200} = (5.38 \pm 0.11) \times 10^{12}$, $c_{200} = 2.4 \pm 0.13$ with a reduced $\chi^2 = 0.6$.

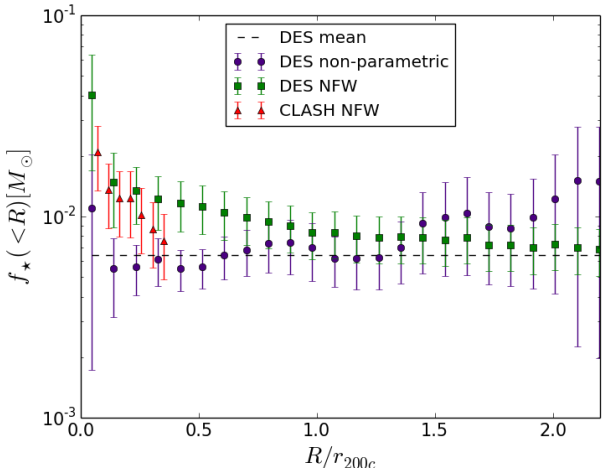

Figure 9. Cumulative radial distribution of the fraction of stellar mass of the galaxies in the cluster as computed in this work over the total mass from lensing studies. For the DES $f_\star$, the total mass comes from the non-parametric reconstruction of the weak lensing shear profile done in Melchior et al. 2015 (purple points), or from their NFW best fit (green squares). For CLASH, M_{tot} is a result of the Umetsu et al. (2015) NFW best-fit for CLASH from a strong lensing, weak lensing and magnification joint analysis (red triangles). The mean DES stellar mass fraction from non-parametric weak lensing mass profile is $f_* = (7.49 \pm 0.39) \times 10^{-3}$, and is represented by the dashed line. The radius R is projected, and rescaled with $r_{200c} = 3.15$ Mpc. Errorbars show the 68% confidence level.

From the DES stellar mass profile and the total matter one (from the aperture mass densiometry), we derive the stellar mass fraction $f_\star(< R) = M_\star(< R)/M_{tot}(< R)$, which is represented by the purple points in Figure 9. Within r_{200c} radius, we find $f_\star^{DES}(< r_{200c}) = (7.0 \pm 2.2) \times 10^{-3}$, compatible within 1σ in the outer regions with the result from Bahcall & Kulier (2014): $f_\star \simeq (1.0 \pm 0.4) \times 10^{-2}$ above $\sim 300h^{-1}$ kpc. In their paper, Bahcall & Kulier (2014) examine the stellar fraction profile by stacking $> 10^5$ SDSS groups and clusters, divided into 3 richness subsamples.[8] Inside r_{200c} we recover a lower stellar mass fraction compared to their work. The discrepancy can be explained in light of the different analyses carried out in Bahcall & Kulier (2014):

- Bahcall & Kulier (2014) stack clusters with different properties and at different redshifts.
- they included the contribution of the diffuse intracluster light (ICL), which increases $f_\star$ by a factor 1.15 within r_{200c}.
- The luminosity profiles and weak lensing mass profiles have been de-projected to obtain 3D profiles in their work. On the other hand, considering the projected $f_\star$ means that we are including the contribution of the cluster outskirts along the line of sight when we look at cluster core. In these regions, the stellar mass fraction is lower, and this tends to reduce 2D $f_\star$ at small radii with respect the 3D behaviour.

[8] They define the richness N_{200} as the number of galaxies in the red sequence with rest-frame i-band luminosity $L_i > 0.4L^*$ located within a radius r_{200}^{gals} from the BCG (i.e. within the radius where the local galaxy overdensity is 200).

On the other hand, the average stellar mass of the Universe, estimated to be $f_{\star,cosmic} = 0.9 \pm 0.1\%$ (as derived in Bahcall & Kulier 2014) is recovered outside r_{200c}, as we would expect even for a projected profile.

Overall, no particular radial trend is found, but it might be hidden by the large errors. In order to reduce the latter, dominated by the weak lensing reconstructed mass, and have a precise estimation of the stellar mass fraction, we will need to apply the same reasoning to a large sample of DES clusters.

If we take the NFW mass profile with the lensing best-fit parameters as total mass in $f_\star$, we get the green points in Figure 11 for DES, and the red ones for CLASH. The higher values towards the centre of the cluster are due to the fact that the function in eq. (6) goes to zero for $R \to 0$, while the BCG stellar mass contributed to $M_\star$ up to very small radii. Moreover, the halo/cusp problem (see e.g. de Blok 2010) is a known problem of the NFW profile and will produce different results from a non-parametric mass profile from weak lensing. Use of the same dark matter halo parameterisation brings the two datasets into agreement at the 1σ level.

5.5 DES Stellar Masses and Weak Lensing Mass Maps

In this section, we explore the correlation between the stellar mass maps and the DES weak lensing mass map by Melchior et al. (2015). Melchior et al. (2015) adopted the aperture-mass technique from Schneider (1996) and computed the map of M_{ap}/σ_{ap} for this cluster, where M_{ap} is the aperture mass and it is defined as the sum of all ellipticity measurements $\epsilon_t(\vartheta_j)$ inside a circular aperture:

$$M_{ap}(\vartheta) = \sum_j Q(|\vartheta - \vartheta_j|)\epsilon_t(\vartheta_j) \ . \tag{8}$$

In eq. (8) Q is a weight function, and the ellipticities are computed with respect to the centre ϑ of the circular aperture. The variance of the aperture mass is given by:

$$\sigma^2_{M_{ap}} = \frac{\sigma^2_\epsilon}{2} \sum_j Q^2(|\vartheta - \vartheta_j|) \ . \tag{9}$$

In Figure 10 we show the DES aperture mass map (black contours) and our stellar mass map (coloured density map) in $30' \times 30'$ around the BCG position. Both maps, have a resolution of $0.4997'$/pixel and have been smoothed with a Gaussian of $\sigma = 1'$.

An elongated structure spanning for ~ 4 Mpc around the BCG is clearly present in both maps, as well as a few clumps lying inside and outside the r_{200c} radius. Note that the mass structures that can be seen in the total mass map may lie outside the cluster but still cause the lensing, as they are along the line of sight, while the DES galaxies considered here, are only those at the cluster redshift. This fact partially explains why the peaks and minima in the stellar mass and aperture mass maps may be not always coincident. Also, the peak of the stellar mass distribution coincides with the BCG position, while the weak lensing map shows a small offset of the peak from the BCG: Gruen et al. (2013) already addressed this effect to the expected shape noise studied by Dietrich et al. (2012).

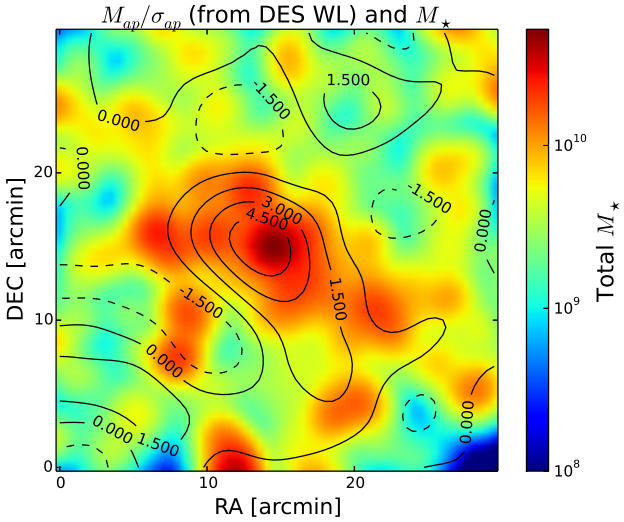

Figure 10. DES total stellar mass distribution (coloured density plot) compared to the mass map (*i.e.* map of M_{ap}/σ_{ap}, in contours) from the weak lensing analysis by Melchior et al. (2015). Both maps have a resolution of $0.4997'$/pixel and have been smoothed with a Gaussian of $\sigma = 1'$.

The correlation that can be seen by eye between M_{ap}/σ_{ap} and $\log M_\star$, is quantified by a Pearson coefficient of $r = 0.30$ when cross-correlating the maps pixel by pixel. Again, the correlation expected between stellar mass and total matter (quantified in this case by the aperture mass and convergence) in a cluster is diminished by the fact that the gravitational lensing gives an integrated information about the mass along the line of sight.

6 CONCLUSIONS

We compared the catalogues derived from DES and CLASH observations of the galaxy cluster RXC J2248.7–4431, treating CLASH as a validation set for DES. Photometric redshifts and stellar masses for both datasets were computed using LePhare, and we found that stellar masses can be estimated with good precision with DES, despite the lower number of bands available. Gravitational lensing results from both DES and CLASH were used to compare stellar and total mass maps, as well as the mass profiles and stellar mass fraction.

We conclude that:

(i) HST data can be used as a validation set for DES data and results. We expect 3 more CLASH clusters to be included in the whole DES footprint. We found that in this case, using the `CLASS_STAR` parameters with the mentioned cut is more efficient than adopting the `SPREAD_MODEL_I` with the cut at 0.003.

(ii) DES photo-zs are compatible with the 17 HST filters photo-zs within the DES requirements. The $z \sim 0.1$ offset observed in the DES photo-zs, is due to a colour-redshift degeneracy that cannot be broken without UV bands at redshifts below 0.4. We found that such offset would percolate into the stellar mass estimates and bias the results by ~ 0.16 dex. In order to perform stellar mass studies, we therefore overcame the problem of the redshift estimation for single cluster members by devising a technique as follows. This method treats separately the red galaxies, as found by RedMaPPer, and the blue galaxies. The redshift information can either be the spectroscopic redshift of the cluster, if available, or the RedMaPPer cluster photometric redshift (as RedMaPPer photo-zs are estimated with high precision). In order to estimate the blue galaxies contribution to the stellar mass, we perform a background subtraction which is only possible thanks to the DECam wide field of view.

(iii) We then estimated total stellar mass and stellar mass fraction profiles for both DES and CLASH, reaching large radii with DES. Within the projected r_{200c} radius, we find a fraction of stellar mass over total mass (derived from weak lensing) $f_\star(< r_{200c}) = (7.0 \pm 2.2) \times 10^{-3}$ with DES, which is compatible with other recent measurements from an independent dataset (Bahcall & Kulier 2014).

(iv) On cosmological scales the ratio of baryon to dark matter densities is $\Omega_b/\Omega_m \approx 16\%$ (e.g. Planck Collaboration et al. 2015). In the cluster core we find that the ratio of stellar mass to dark matter is 0.7%. This means that if the cluster distribution is representative, than only 4% of the baryons are locked into stars (compatible within 2σ with Fukugita & Peebles 2004).

(v) The stellar mass fraction profiles we derive from DES and CLASH are compatible within 1σ, provided that the same parametrisation is used for the dark matter halo profile.

(vi) HST clusters can be used to test and calibrate stellar mass estimates. In future works we plan to test the stellar mass to light ratio derived from DES to that from HST, as this should be nominally invariant under changes in galaxy apertures (that are different between the two datasets used in this work), and therefore better matched than $M_\star$ between the surveys. In addition, an extensive spectroscopic

campaign carried out with the Very Large Telescope (VLT) (CLASH–VLT, Rosati et al. 2014) is currently providing thousands of spectra for 14 CLASH clusters. In the future, we plan to use this survey to further test our technique: this dataset will include spectra up to very large cluster radii, making CLASH–VLT ideal to test stellar masses on the large scales explored by DES. CLASH–VLT analysis of stellar masses for the cluster RXJ2248 are in course of preparations (Annunziatella et al., in prep.), and stellar mass density profiles have been studied recently (Annunziatella et al. 2014, Annunziatella et al. 2015).

(vii) In the future, we plan to apply the same techniques to a sample of 100 000 stacked DES clusters and deduce important information about galaxy evolution by looking at the relation between stellar and total mass, as a function of radii and redshift, at the Stellar Mass Function and at the stellar mass environment dependence. The stacking of the whole DES sample would allow us to estimate $f_\star$ with an error significantly smaller than what is given here.

ACKNOWLEDGMENTS

A. Palmese acknowledges the UCL PhD studentship. O. Lahav acknowledges support from a European Research Council Advanced Grant FP7/291329, which also supported M. Banerji and S. Jouvel.
D. Gruen and S. Seitz were supported by SFB-Transregio 33 "The Dark Universe" by the Deutsche Forschungsgemeinschaft (DFG) and the DFG cluster of excellence 'Origin and Structure of the Universe'. D. Gruen was also supported by NASA through the Einstein Fellowship Program, grant PF5-160138.
T. Jeltema acknowledges support from the DOE grant DE-SC0013541.
This work has benefitted by data taken by the CLASH collaboration.
A. Palmese and O. Lahav acknowledge N. Bahcall and M. Milgrom for stimulating discussions about this work.
Funding for the DES Projects has been provided by the U.S. Department of Energy, the U.S. National Science Foundation, the Ministry of Science and Education of Spain, the Science and Technology Facilities Council of the United Kingdom, the Higher Education Funding Council for England, the National Center for Supercomputing Applications at the University of Illinois at Urbana-Champaign, the Kavli Institute of Cosmological Physics at the University of Chicago, the Center for Cosmology and Astro-Particle Physics at the Ohio State University, the Mitchell Institute for Fundamental Physics and Astronomy at Texas A&M University, Financiadora de Estudos e Projetos, Fundação Carlos Chagas Filho de Amparo à Pesquisa do Estado do Rio de Janeiro, Conselho Nacional de Desenvolvimento Científico e Tecnológico and the Ministério da Ciência, Tecnologia e Inovação, the Deutsche Forschungsgemeinschaft and the Collaborating Institutions in the Dark Energy Survey.

The Collaborating Institutions are Argonne National Laboratory, the University of California at Santa Cruz, the University of Cambridge, Centro de Investigaciones Energéticas, Medioambientales y Tecnológicas-Madrid, the University of Chicago, University College London, the DES-Brazil Consortium, the University of Edinburgh, the Eidgenössische Technische Hochschule (ETH) Zürich, Fermi National Accelerator Laboratory, the University of Illinois at Urbana-Champaign, the Institut de Ciències de l'Espai (IEEC/CSIC), the Institut de Física d'Altes Energies, Lawrence Berkeley National Laboratory, the Ludwig-Maximilians Universität München and the associated Excellence Cluster Universe, the University of Michigan, the National Optical Astronomy Observatory, the University of Nottingham, The Ohio State University, the University of Pennsylvania, the University of Portsmouth, SLAC National Accelerator Laboratory, Stanford University, the University of Sussex, and Texas A&M University.

The DES data management system is supported by the National Science Foundation under Grant Number AST-1138766. The DES participants from Spanish institutions are partially supported by MINECO under grants AYA2012-39559, ESP2013-48274, FPA2013-47986, and Centro de Excelencia Severo Ochoa SEV-2012-0234. Research leading to these results has received funding from the European Research Council under the European Unions Seventh Framework Programme (FP7/2007-2013) including ERC grant agreements 240672, 291329, and 306478.

REFERENCES

Abell G. O., Corwin, Jr. H. G., Olowin R. P., 1989, Astrophys.J., 70, 1
Acquaviva V., Raichoor A., Gawiser E., 2015, Astrophys.J., 804, 8
Annunziatella M. et al., 2014, Astrophys.J., 571, A80
Annunziatella M. et al., 2015, ArXiv e-prints
Arnouts S., Cristiani S., Moscardini L., Matarrese S., Lucchin F., Fontana A., Giallongo E., 1999, Mon.Not.Roy.Astron.Soc., 310, 540
Bahcall N. A., Kulier A., 2014, Mon.Not.Roy.Astron.Soc., 439, 2505
Banerji M. et al., 2013, Mon.Not.Roy.Astron.Soc., 431, 2209
Benítez N. et al., 2004, Astrophys.J., 150, 1
Bertin E., Arnouts S., 1996, Astronomy and Astrophysics Supplement, 117, 393
Bertin E., Arnouts S., 2010
Böhringer H. et al., 2004, Astrophys.J., 425, 367
Bonnett C. et al., 2015, ArXiv e-prints
Bouy H., Bertin E., Moraux E., Cuillandre J.-C., Bouvier J., Barrado D., Solano E., Bayo A., 2013, Astrophys.J., 554, A101
Bruzual G., Charlot S., 2003, Mon.Not.Roy.Astron.Soc., 344, 1000
Calzetti D., Armus L., Bohlin R. C., Kinney A. L., Koornneef J., et al., 2000, Astrophys.J., 533, 682
Chabrier G., 2003, Publ.Astron.Soc.Pac., 115, 763
Conroy C., 2013, Annual Review of Astronomy and Astrophysics, 51, 393
Crocce M. et al., 2015, ArXiv e-prints
de Blok W. J. G., 2010, Advances in Astronomy, 2010, 789293
Desai S. et al., 2012, Astrophys.J., 757, 83
Diehl H. T. et al., 2014, in Society of Photo-Optical Instrumentation Engineers (SPIE) Conference Series, Vol.

9149, Society of Photo-Optical Instrumentation Engineers (SPIE) Conference Series, p. 91490V
Dietrich J. P., Böhnert A., Lombardi M., Hilbert S., Hartlap J., 2012, Mon.Not.Roy.Astron.Soc., 419, 3547
Eisenstein D. J. et al., 2001, Astrophys.J., 122, 2267
Flaugher B. et al., 2015, Astrophys.J., 150, 150
Fukugita M., Peebles P. J. E., 2004, Astrophys.J., 616, 643
Gómez P. L. et al., 2012, Astrophys.J., 144, 79
Górski K. M., Hivon E., Banday A. J., Wandelt B. D., Hansen F. K., Reinecke M., Bartelmann M., 2005, Astrophys.J., 622, 759
Gruen D., Brimioulle F., Seitz S., Lee C. H., Young J., et al., 2013, Mon.Not.Roy.Astron.Soc., 432, 2
Ilbert O. et al., 2006, Astrophys.J., 457, 841
Ilbert O. et al., 2009, Astrophys.J., 690, 1236
Ilbert O. et al., 2010, Astrophys.J., 709, 644
Jouvel S. et al., 2014, Astrophys.J., 562, A86
Koekemoer A. M. et al., 2011, Astrophys.J., 197, 36
Koekemoer A. M., Fruchter A. S., Hook R. N., Hack W., 2002, 337
Maughan B. J., Jones C., Forman W., Van Speybroeck L., 2008, Astrophys.J., 174, 117
Melchior P. et al., 2015, Mon.Not.Roy.Astron.Soc., 449, 2219
Meneghetti M., Rasia E., Merten J., Bellagamba F., Ettori S., Mazzotta P., Dolag K., Marri S., 2010, Astrophys.J., 514, A93
Mohr J. J. et al., 2012, 8451, 0
Monna A. et al., 2014, Mon.Not.Roy.Astron.Soc., 438, 1417
Navarro J. F., Frenk C. S., White S. D. M., 1996, Astrophys.J., 462, 563
Oaxaca Wright C., Brainerd T. G., 1999, ArXiv Astrophysics e-prints
Planck Collaboration et al., 2015, ArXiv e-prints
Postman M. et al., 2012, Astrophys.J., 199, 25
Rosati P. et al., 2014, The Messenger, 158, 48
Rozo E., Rykoff E. S., Becker M., Reddick R. M., Wechsler R. H., 2014, ArXiv e-prints
Rykoff E. S. et al., 2014, Astrophys.J., 785, 104
Sánchez C. et al., 2014, Mon.Not.Roy.Astron.Soc., 445, 1482
Schneider P., 1996, Mon.Not.Roy.Astron.Soc., 283, 837
Sevilla I. et al., 2011, ArXiv e-prints
Soumagnac M. T. et al., 2013, ArXiv e-prints
Suchyta E. et al., 2015, ArXiv e-prints
Swanson M. E. C., Tegmark M., Hamilton A. J. S., Hill J. C., 2008, Mon.Not.Roy.Astron.Soc., 387, 1391
The Dark Energy Survey Collaboration, 2005, ArXiv Astrophysics e-prints
Umetsu K., Zitrin A., Gruen D., Merten J., Donahue M., Postman M., 2015, ArXiv e-prints
Zhang Y., McKay T. A., Bertin E., Jeltema T., Miller C. J., Rykoff E., Song J., 2014, ArXiv e-prints

APPENDIX A: MAGNITUDE COMPARISON

Considering only those matched sources with a signal to noise ratio $S/N > 10$ in the DES i-band, excluding stars and objects with SExtractor `FLAGS` > 3 (in order to exclude objects with saturated pixels or corrupted data, but include objects that were initially blended) we are left with 327 sources observed in the g and r bands, and 331 in the i and z bands. The differences $\Delta_{\rm m} = m_{\rm DES} - m_{\rm CLASH}$ are plotted in Figure A1, as well as the DES magnitudes as a function of the CLASH ones for the matched sources. The magnitudes plotted are SExtractor isophotal magnitudes `MAG_ISO` for both DES and CLASH. $\Delta_{\rm m}$ in the $griz$ bands has been corrected for the magnitude shifts due to the differences between these DES and HST filters. The offset has been computed using two"extreme case" SED templates (one elliptical, one irregular) at the cluster redshift. We have not taken into consideration the Y band offset as the HST and DES filters are too different.

Figure A1 shows an offset in the DES magnitudes, especially in the gri bands, which my be due to different choices of threshold or background when running SExtractor. Nevertheless the linear trend is clear, bringing to Pearson coefficients between 0.91 and 0.98 in all bands. The higher scatter that we could expect in the Y band (as the corresponding CLASH filter is the F105W, which is much more spread towards the infrared than the DES Y filter) is actually compensated for by higher DES photometric errors. The mean difference in magnitude Δm between the two datasets is 0.13, 0.04, -0.07, -0.07 and 0.08 in the $grizY$ bands respectively.

APPENDIX B: PHOTO-Z CONSISTENCY TEST

We have tested whether the fact that we assumed a photo-z that was computed with a certain set of templates to then compute the stellar mass with a larger set of templates is consistent. With photometric surveys data, it is a common method to perform estimation of the photometric redshift and SED fitting in two steps, which involve fixing the redshift of a galaxy at the best fit value obtained in the first step. Although this may not be the most elegant way of solving the problem of the lack of spectroscopic information, it has been proven to lead to only a small bias in the SED fitting parameters, when compared to results given by the simultaneous estimation of redshift and stellar mass (see Acquaviva, Raichoor & Gawiser 2015). Moreover, here we can take advantage of the prior information that this is a cluster.

In order to do test the consistency of the photo-z choice, we want to show that the resulting photo-z is not drastically dependent on the choice of templates. Therefore, we compare the photo-zs given by Le Phare when using the COSMOS templates and the BC03 ones. A comparison is shown in Figure B1 for all the galaxies in the DES field of view. We retrieve that 71% of the galaxies have $|\Delta z| = |z_{BC03} - z_{COSMOS}| < 0.12$.

This paper has been typeset from a TEX/ LATEX file prepared by the author.

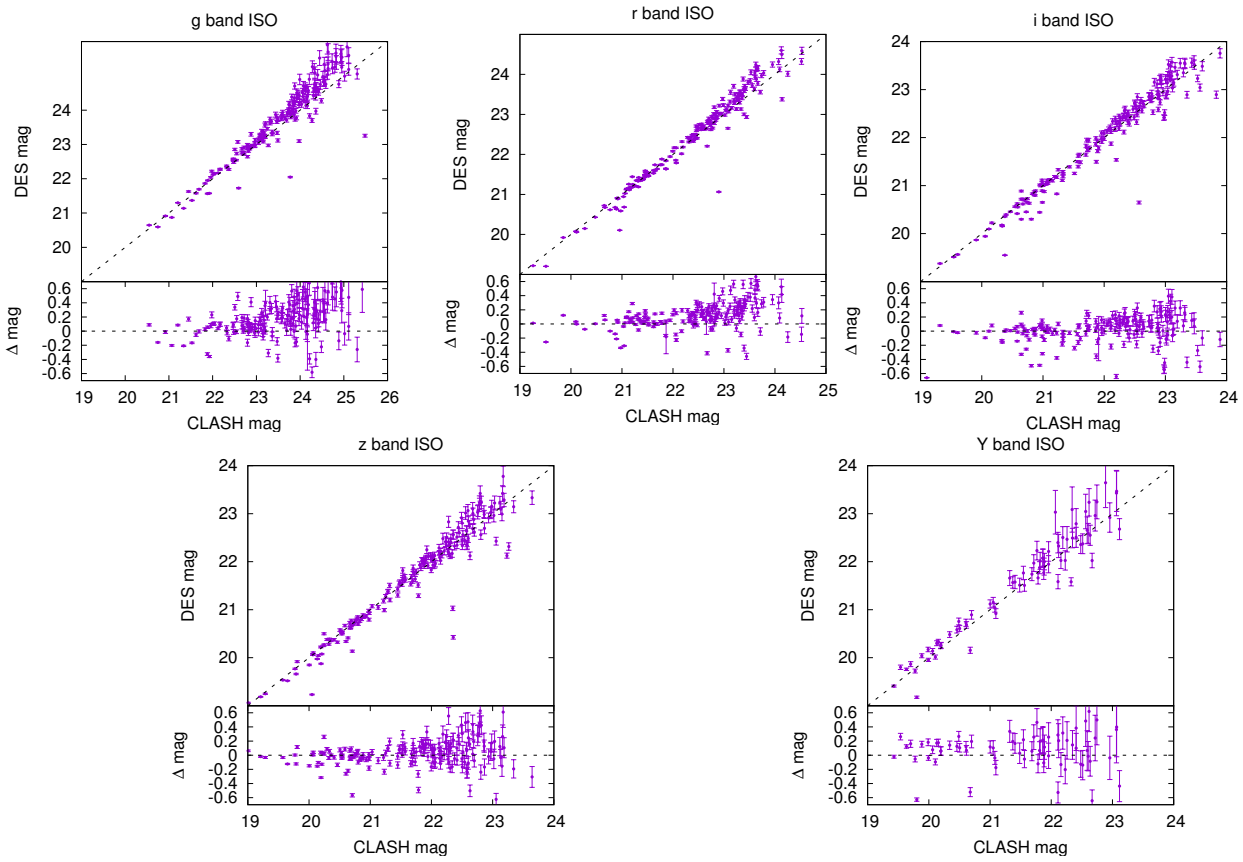

Figure A1. DES magnitues compared to CLASH magnitudes, with bottom plots of $\Delta_{\rm m} = m_{\rm CLASH} - m_{\rm DES}$ in the g,r,i and z bands for the matched sources that satisfy $S/N > 10$ and filtering the sources with `FLAGS`> 3. CLASH errorbars are not plotted for visualisation purposes, while those on the DES magnitudes represent the 1σ error. The dashed black lines represent the ideal case $m_{\rm CLASH} = m_{\rm DES}$.

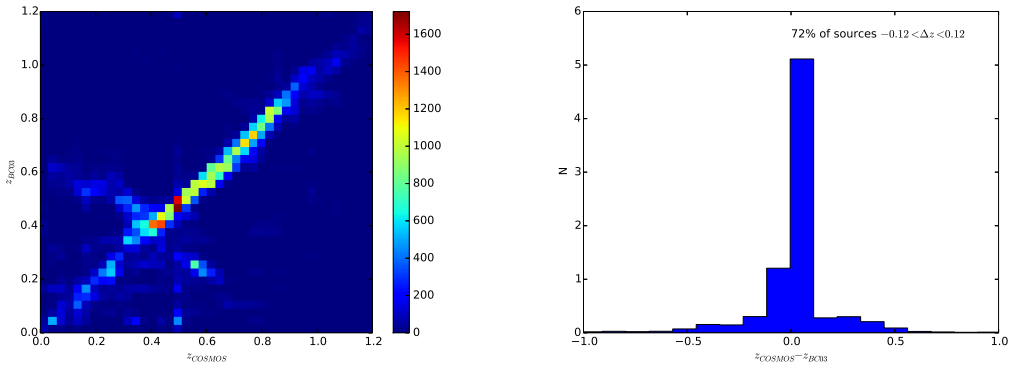

Figure B1. *Upper panel*: Comparison of the photo-zs computed using the Bruzual and Charlot 2003 templates and those using the COSMOS templates. *Lower panel:* Residuals of the photo-zs computed using the two differnt set of templates.

[1]Department of Physics and Astronomy, University College London, London, UK
[2]Institute of Astronomy, University of Cambidge, Madingley Road, Cambridge, UK
[3]SLAC National Accelerator Laboratory, Menlo Park, CA 94025, USA
[4]Kavli Institute for Particle Astrophysics & Cosmology, P. O. Box 2450, Stanford University, Stanford, CA 94305, USA
[5]University Observatory Munich, Scheinerstrasse 1, 81679 Munich, Germany
[6]Max Planck Institute for Extraterrestrial Physics, Giessenbachstrasse, 85748 Garching, Germany
[7]Department of Astrophysical Sciences, Princeton University, Princeton, NJ 08544, USA
[8]Institut de Física d'Altes Energies (IFAE), The Barcelona Institute of Science and Technology, Campus UAB, 08193 Bellaterra (Barcelona) Spain

[9]Fermi National Accelerator Laboratory, Batavia, IL 60510, USA
[10]Department of Physics, University of California, Santa Cruz, CA 95064 USA
[11]Department of Physics and Astronomy, Pevensey Building, University of Sussex, Brighton, BN1 9QH, UK
[12]Department of Physics, University of Arizona, Tucson, AZ 85721, USA
[13]Department of Physics and Astronomy, University of Pennsylvania, Philadelphia, PA 19104, USA
[14]Physics Department, University of Michigan, 450 Church Street, Ann Arbor, MI, 48109, USA
[15]Cerro Tololo Inter-American Observatory, National Optical Astronomy Observatory, Casilla 603, La Serena, Chile
[16]Department of Physics and Electronics, Rhodes University, PO Box 94, Grahamstown, 6140, South Africa
[17]CNRS, UMR 7095, Institut d'Astrophysique de Paris, F-75014, Paris, France
[18]Sorbonne Universités, UPMC Univ Paris 06, UMR 7095, Institut d'Astrophysique de Paris, F-75014, Paris, France
[19]Institute of Cosmology & Gravitation, University of Portsmouth, Portsmouth, PO1 3FX, UK
[20]Laboratório Interinstitucional de e-Astronomia - LIneA, Rua Gal. José Cristino 77, Rio de Janeiro, RJ - 20921-400, Brazil
[21]Observatório Nacional, Rua Gal. José Cristino 77, Rio de Janeiro, RJ - 20921-400, Brazil
[22]Department of Astronomy, University of Illinois, 1002 W. Green Street, Urbana, IL 61801, USA
[23]National Center for Supercomputing Applications, 1205 West Clark St., Urbana, IL 61801, USA
[24]Institut de Ciències de l'Espai, IEEC-CSIC, Campus UAB, Carrer de Can Magrans, s/n, 08193 Bellaterra, Barcelona, Spain
[25]School of Physics and Astronomy, University of Southampton, Southampton, SO17 1BJ, UK
[26]Excellence Cluster Universe, Boltzmannstr. 2, 85748 Garching, Germany
[27]Faculty of Physics, Ludwig-Maximilians University, Scheinerstr. 1, 81679 Munich, Germany
[28]Department of Astronomy, University of Michigan, Ann Arbor, MI 48109, USA
[29]Kavli Institute for Cosmological Physics, University of Chicago, Chicago, IL 60637, USA
[30]Department of Astronomy, University of California, Berkeley, 501 Campbell Hall, Berkeley, CA 94720, USA
[31]Lawrence Berkeley National Laboratory, 1 Cyclotron Road, Berkeley, CA 94720, USA
[32]Center for Cosmology and Astro-Particle Physics, The Ohio State University, Columbus, OH 43210, USA
[33]Department of Physics, The Ohio State University, Columbus, OH 43210, USA
[34]Australian Astronomical Observatory, North Ryde, NSW 2113, Australia
[35]George P. and Cynthia Woods Mitchell Institute for Fundamental Physics and Astronomy, and Department of Physics and Astronomy, Texas A&M University, College Station, TX 77843, USA
[36]Departamento de Física Matemática, Instituto de Física, Universidade de São Paulo, CP 66318, CEP 05314-970, São Paulo, SP, Brazil
[37]Institució Catalana de Recerca i Estudis Avançats, E-08010 Barcelona, Spain
[38]Jet Propulsion Laboratory, California Institute of Technology, 4800 Oak Grove Dr., Pasadena, CA 91109, USA
[39]Centro de Investigaciones Energéticas, Medioambientales y Tecnológicas (CIEMAT), Madrid, Spain
[40]Vikram,Vinu,V. Vikram,True,"Argonne National Laboratory, 9700 South Cass Avenue, Lemont, IL 60439, USA